Journal of Applied Mechanics. Received December 05, 2025;
Accepted manuscript posted January 12, 2026. doi:10.1115/1.4070821

JAM-25-1433

Three-node torsional spring element formulation for the analysis of reconfigurable bar-linked structures

Hardik Y. Patil*
Civil and Environmental Engineering,
University of Michigan,
Ann Arbor, Michigan 48109, USA
Email: hardikyp@umich.edu

Evgueni T. Filipov
Civil and Environmental Engineering,
Mechanical Engineering,
University of Michigan,
Ann Arbor, Michigan 48109, USA
Email: filipov@umich.edu

ABSTRACT

This technical note presents the derivation, validation, and application of a three-node torsional spring (3NTS) *element for the analysis of bar-linked, reconfigurable structures. The 3NTS element assigns rotational stiffness to a joint (node) of two axial force members (bars) in truss-like assemblies. This element avoids the use of rotational degrees of freedom in the model by recasting its resisting moment into equivalent nodal forces, which are consistent with global equilibrium, thereby keeping the model size compact and computationally efficient. The 3NTS is integrated into standard nonlinear solvers to simulate large-displacement response and validated against analytical solutions of two benchmark examples: the simplest 3NTS structure and the buckling of a vertical column. We further apply the framework to a reconfigurable truss structure from our previous work to illustrate potential functional use cases and outline its broader applicability to metamaterials, kirigami systems, and biomechanical assemblies. An open-source matrix structural analysis tool implementing the 3NTS and axial force members is made available with this note.*

*Corresponding author

Keywords: Torsional spring element; Joint rotational stiffness; Reconfigurable bar-linked structures

1 INTRODUCTION

Over the past century, structural element formulations have evolved to capture nonlinearity and connection flexibility, enabling accurate modeling of practical structures [1]. However, the support for modeling joint rotational stiffness within truss-like structures using a torsional (or coil) spring remains limited, especially in formulations with minimal degrees of freedom (DOF) and high computational efficiency.

Joint rotational stiffness is crucial in applications where controlled joint rotation influences the global structural behavior. Some examples include reconfigurable linkages and robotic arms that rely on programmed hinge stiffnesses [2, 3, 4, 5], biomechanics where joint stiffness affects function [6, 7], origami-inspired mechanisms where crease stiffness governs panel folding [8, 9, 10], and semi-rigid connections in lattice structures and metamaterials that store and release energy to achieve functional reconfiguration [11, 12, 13].

A typical workaround for joint rotational stiffness in two-dimensional bar-linked structures involves the use of semi-rigid joints. These semi-rigid joints introduce a short beam element (3 DOFs per node) at the joint and impose rotational stiffness by assigning ad-hoc stiffness values to the node's rotational degree of freedom [14, 15, 16, 17]. While serviceable, this approach may yield spurious results if the user-chosen stiffness value is not representative of the structural behavior [18]. Furthermore, it increases the computational complexity by inflating the model, as representing a single joint by a beam segment requires six DOFs over the two required for a bar-bar joint in two-dimensional space.

We address this gap by introducing a *three-node torsional spring (3NTS)* element to model a joint's rotational resistance within bar-linked structures. The 3NTS element consists of two elastic axial force members (bars) joined at an intermediate node, which hosts a torsional spring of lumped rotational stiffness K_T [Nm/rad] (Fig. 1). When the relative angle between the bars (α) changes, the spring develops a resisting moment that is recast as equivalent nodal forces con-

sistent with global equilibrium. Since α is a function of the coordinates of the three nodes, the 3NTS requires only six translational DOFs for its representation in a two-dimensional space. Consequently, a two-dimensional bar-linked assembly using the 3NTS elements has the *same* global DOF count as an equivalent spring-less truss structure. Thus, by avoiding rotational DOFs, this formulation yields a compact model with improved computational efficiency over ad-hoc joint rotational stiffness workarounds.

The proposed 3NTS element provides a minimal, first-principles representation of a joint with rotational stiffness, which the current literature lacks. Furthermore, it decouples the joint's moment-rotation behavior from axial force-displacement effects by allowing standard bar elements to handle the axial and positional effects. This concept draws on the bar and hinge origami models [19, 20, 21, 22] where three-dimensional rotational hinges capture crease folding and sheet bending. Here, we distill that concept and apply it to a two-dimensional case to assess the global structural behavior of bar-linked reconfigurable structures with torsional springs. We believe that this reduced-order formulation will aid in the exploration and efficient simulation of system behaviors in biomechanics, robotics, compliant mechanisms, planar metamaterials, and kirigami lattices.

The remainder of the note is organized as follows. Section 2 derives the torsional spring stiffness matrix. Section 3 validates the simulated response of the torsional spring against analytical solutions of benchmark examples. Section 4 illustrates the potential application of the developed analysis program to reconfigurable bar-linked structures. Finally, Section 5 summarizes the contributions of this work.

2 STIFFNESS MATRIX OF A THREE-NODE TORSIONAL SPRING ELEMENT

The stiffness matrix of a two-dimensional three-node torsional spring is derived from constitutive law by evaluating the Jacobian and Hessian of its strain energy. The torsional spring unit shown in Fig. 1 consists of three nodes 1, 2, and 3 with undeformed coordinates (X_1, Y_1), (X_2, Y_2), and (X_3, Y_3), respectively. Bar 1 connects nodes 1 and 2, and bar 2 connects nodes 2 and 3. Each bar behaves as an axial-force member. A torsional spring of stiffness K_T is located at node 2, producing a moment only when the relative angle between bars 1 and 2 changes. The nodal

Journal of Applied Mechanics. Received December 05, 2025;
Accepted manuscript posted January 12, 2026. doi:10.1115/1.4070821

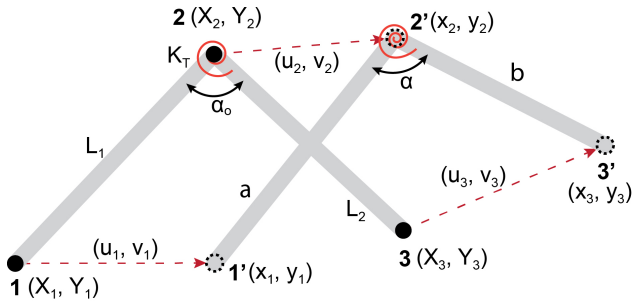

Fig. 1. A schematic representation of the three-node rotational spring unit depicting the nodal displacements

coordinates in the deformed configuration are (x_1, y_1), (x_2, y_2) and (x_3, y_3).

Let the position vectors in the undeformed and deformed configurations be $R_1 = [X_1,\ Y_1]^\top$, $R_2 = [X_2,\ Y_2]^\top$, $R_3 = [X_3,\ Y_3]^\top$, and $r_1 = [x_1,\ y_1]^\top$, $r_2 = [x_2,\ y_2]^\top$, $r_3 = [x_3,\ y_3]^\top$, respectively. The global nodal coordinate vectors are expressed as $R = [R_1^\top,\ R_2^\top,\ R_3^\top]^\top$ and $r = [r_1^\top,\ r_2^\top,\ r_3^\top]^\top$, and the corresponding displacement vector is defined as $u = r - R$.

2.1 Torsional spring constitutive law

The strain energy of a linearly elastic three-node torsional spring is expressed as

$$U(\alpha) = \frac{1}{2} K_T (\alpha - \alpha_o)^2 \ , \tag{1}$$

where K_T is the spring's rotational stiffness, $\alpha = \alpha(r)$ denotes the relative angle between the two connected bars as a function of the global nodal coordinate vector r, and $\alpha_o = \alpha(R)$ represents the undeformed (rest) angle of the spring, defined with respect to the undeformed global nodal coordinate vector R.

The internal nodal force vector is obtained by differentiating the strain energy with respect to the displacement vector:

$$F_{\text{int}} = \frac{\partial U}{\partial u} = \frac{\partial U}{\partial \alpha} \frac{\partial \alpha}{\partial u} \ . \tag{2}$$

Recalling that the reference configuration of the spring R is constant, gradients with respect to the displacement vector are equivalent to those with respect to the deformed coordinates, i.e., $\partial u = \partial r$. Defining the gradient of the relative angle as $\nabla\alpha = \partial\alpha/\partial u = \partial\alpha/\partial r$ and the moment generated by the spring as $M = \partial U/\partial\alpha = K_T(\alpha - \alpha_o)$, the internal force can be expressed as

$$F_{\text{int}} = M\nabla\alpha = K_T(\alpha - \alpha_o)\nabla\alpha \ . \tag{3}$$

The tangent stiffness matrix is obtained by differentiating the internal force with respect to the deformed global nodal coordinates:

$$K_{\text{spr}} = \frac{\partial F_{\text{int}}}{\partial r} = \frac{\partial}{\partial r}\left(M(r)\nabla\alpha(r)\right) = M(r)\nabla^2\alpha(r) + \nabla M(r)\nabla\alpha(r)^\top \tag{4}$$

Because $M = K_T(\alpha - \alpha_o)$, it follows that $\nabla M = K_T\nabla\alpha$. Substituting these relations into Eq. 4 yields the final expression for the spring element stiffness matrix:

$$K_{\text{spr}} = K_T\left[(\nabla\alpha)(\nabla\alpha)^\top + (\alpha - \alpha_o)\nabla^2\alpha\right] \ . \tag{5}$$

2.2 Relative angle between the bars

Let the vectors along bars 1 and 2 be defined as $a = r_1 - r_2$ and $b = r_3 - r_2$, where $r_i = [x_i, y_i]^\top$ are the nodal position vectors in the deformed configuration. Define the 90° clockwise rotation matrix N such that, for any vector v , the product Nv represents a rotation of v by $+90°$. Furthermore, the property $N = -N^\top$ holds true.

$$N = \begin{bmatrix} 0 & -1 \\ 1 & 0 \end{bmatrix} \tag{6}$$

The cosine and sine of the relative angle α between bars 1 and 2 are then expressed as

$$C = a \cdot b = \|a\| \, \|b\| \, cos(\alpha) \; ,$$
$$S = a^{\top} N b = \|a\| \, \|b\| \, sin(\alpha) \; . \tag{7}$$

Hence, the relative angle α is obtained as

$$\alpha = \tan^{-1} \left(\frac{S}{C} \right) \; . \tag{8}$$

It is important to note that this expression when programmed into MATLAB does not capture the spring's full range of rotation, as the `atan2` function returns values in the interval $[-\pi, \, \pi]$. To obtain a continuous measure of rotation in the range $[0, \, 2\pi)$, the computed angle in MATLAB is modified as

$$\alpha = \mathrm{mod} \left(\alpha, 2\pi \right) \; , \tag{9}$$

where `mod` function returns the remainder after dividing α by 2π. This treatment assumes that the torsional spring does not undergo self-overlapping deformations.

2.3 Derivatives of bar vectors and auxiliary quantities

The gradient of α with respect to the global nodal coordinates can be derived by differentiating Eq. (8). Using the chain rule, we have

$$\nabla \alpha = \frac{1}{1 + (S/C)^2} \left(\frac{C \nabla S - S \nabla C}{C^2} \right) = \frac{C \nabla S - S \nabla C}{C^2 + S^2} = \frac{C \nabla S - S \nabla C}{\|a\|^2 \|b\|^2} \; . \tag{10}$$

To evaluate Eq. (10), the derivatives of vectors a, b, and the scalar quantities C and S with respect to the nodal coordinates are required. These are given by

$$\begin{aligned}
&\frac{\partial a}{\partial r_1} = \mathbf{I} && \frac{\partial a}{\partial r_2} = -\mathbf{I} && \frac{\partial a}{\partial r_3} = \mathbf{0} \\
&\frac{\partial b}{\partial r_1} = \mathbf{0} && \frac{\partial b}{\partial r_2} = -\mathbf{I} && \frac{\partial b}{\partial r_3} = \mathbf{I} \\
&\frac{\partial C}{\partial r_1} = b && \frac{\partial C}{\partial r_2} = -(a+b) && \frac{\partial C}{\partial r_3} = a \\
&\frac{\partial S}{\partial r_1} = Nb && \frac{\partial S}{\partial r_2} = N(a-b) && \frac{\partial S}{\partial r_3} = -Na
\end{aligned} \tag{11}$$

2.4 Closed-form expression for gradient of relative angle

Substituting Eq. (11) into Eq. (10) and applying the vector identity $(x \cdot y)Ny - (x^\top Ny)y = \|y\|^2 Nx$ the gradient components of α can be expressed in compact form as:

$$\begin{aligned}
\nabla\alpha_{11} &= \frac{\partial \alpha}{\partial r_1} = \frac{C(\partial S/\partial r_1) - S(\partial C/\partial r_1)}{\|a\|^2\|b\|^2} = \frac{(a\cdot b)Nb - (a^\top Nb)b}{\|a\|^2\|b\|^2} = \frac{Na}{\|a\|^2} \\
\nabla\alpha_{21} &= \frac{\partial \alpha}{\partial r_2} = \frac{C(\partial S/\partial r_2) - S(\partial C/\partial r_2)}{\|a\|^2\|b\|^2} = \frac{(a\cdot b)N(a-b) + (a^\top Nb)(a+b)}{\|a\|^2\|b\|^2} = \frac{Nb}{\|b\|^2} - \frac{Na}{\|a\|^2} \\
\nabla\alpha_{31} &= \frac{\partial \alpha}{\partial r_3} = \frac{C(\partial S/\partial r_3) - S(\partial C/\partial r_3)}{\|a\|^2\|b\|^2} = \frac{(a\cdot b)(-Na) - (a^\top Nb)a}{\|a\|^2\|b\|^2} = -\frac{Nb}{\|b\|^2}
\end{aligned} \tag{12}$$

These three 2×1 vectors together form the full 6×1 gradient vector $\nabla\alpha$.

2.5 Hessian of the relative angle

The Hessian matrix $\nabla^2\alpha$ is of size 6×6 and consists of nine 2×2 sub-blocks corresponding to the second derivatives of α with respect to the nodal coordinates. The sub-blocks are expressed

as

$$
\begin{aligned}
\mathbf{H}_{11} &= \frac{1}{\|a\|^2}N - \frac{2}{\|a\|^4}(Na)a^\top \\
\mathbf{H}_{22} &= \frac{1}{\|a\|^2}N - \frac{2}{\|a\|^4}(Na)a^\top + \frac{2}{\|b\|^4}(Nb)b^\top - \frac{1}{\|b\|^2}N \\
\mathbf{H}_{33} &= \frac{2}{\|b\|^4}(Nb)b^\top - \frac{1}{\|b\|^2}N \\
\mathbf{H}_{12} &= \mathbf{H}_{21}^\top = \frac{2}{\|a\|^4}(Na)a^\top - \frac{1}{\|a\|^2}N \\
\mathbf{H}_{13} &= \mathbf{H}_{31}^\top = \mathbf{0} \\
\mathbf{H}_{23} &= \mathbf{H}_{32}^\top = \frac{1}{\|b\|^2}N - \frac{2}{\|b\|^4}(Nb)b^\top
\end{aligned}
\tag{13}
$$

Thus, we have all the necessary information to form the stiffness matrix for a three-node torsional spring and use it in matrix structural analysis solvers.

3 VALIDATION OF THE THREE-NODE TORSIONAL SPRING ELEMENT

In this section, we validate the derived stiffness matrix of the torsional spring element by comparing the simulated behavior of two torsional-spring fitted bar-linked structures with their respective analytical solutions. The torsional spring element is implemented alongside linearly elastic axial bar elements within nonlinear structural analysis solvers [23] to facilitate large-deformation simulations of torsional-spring fitted bar-linked structures. The two examples presented herein demonstrate the element's capability to simulate large-deformation responses, evaluate strain energies stored in each structural element, and reproduce buckling behavior in collinear bar systems under compression.

3.1 Comparing analytical and simulated behavior of the simplest three-node torsional spring structure

The simplest bar-linked structure with a three-node torsional spring is the element itself, as shown in Fig. 2 (a). Nodes A and B are fixed supports, while node C is free. Bars connecting

nodes A-B and B-C have a Young's modulus $E = 3 \times 10^6$ Pa, cross-sectional area $A = 0.5$ m^2, and length $L = 1$ m. A torsional spring with stiffness $K_T = 50$ Nm/rad is located at node B. A gradually increasing external load P is applied at node C in the positive Y-direction.

The analytical response of this structure can be obtained using potential energy analysis. When subjected to the applied load P, the bar connecting nodes B and C rotates by an angle θ and elongates by ΔL. The elongation is induced by the component of the applied load along the bar's axis and is expressed as $\Delta L = (PL/EA)\sin(\theta)$. In this deformed state, the total potential energy of the structure is

$$U = \frac{1}{2}K_T\theta^2 - PL\sin(\theta) - \frac{P^2L}{2EA}\sin^2(\theta) + \text{constant}\,. \tag{14}$$

The equilibrium condition is obtained by setting $\partial U/\partial\theta = 0$, which yields the following expression for the applied load P:

$$P = \frac{-AEL\cos(\theta) \pm AE\sqrt{\frac{L\cos(\theta)}{EA}\left(4K_T\theta\sin(\theta) + AEL\cos(\theta)\right)}}{2L\sin\theta\cos\theta}\,. \tag{15}$$

The corresponding vertical displacement of node C due to the applied load becomes $\Delta = (L + \Delta L)\sin(\theta)$.

Figure 2 (b) compares the analytical and simulated load-displacement responses of the simple three-node torsional spring structure. The two curves show excellent agreement over the entire range of deformation. The load increases from zero and appears to approach infinity asymptotically as the bar rotates from 0° to 90°. In reality, the load does not become infinite. Throughout the range of deformation, the applied load is primarily resisted by the torsional spring. As the angular rotation of the bar approaches 90°, however, the load begins to increase approximately in proportion to the axial stiffness of the bar, EA/L, as both the bar and the spring resist the external load. Because this axial stiffness is several orders of magnitude greater than the torsional spring stiff-

Journal of Applied Mechanics. Received December 05, 2025;
Accepted manuscript posted January 12, 2026. doi:10.1115/1.4070821

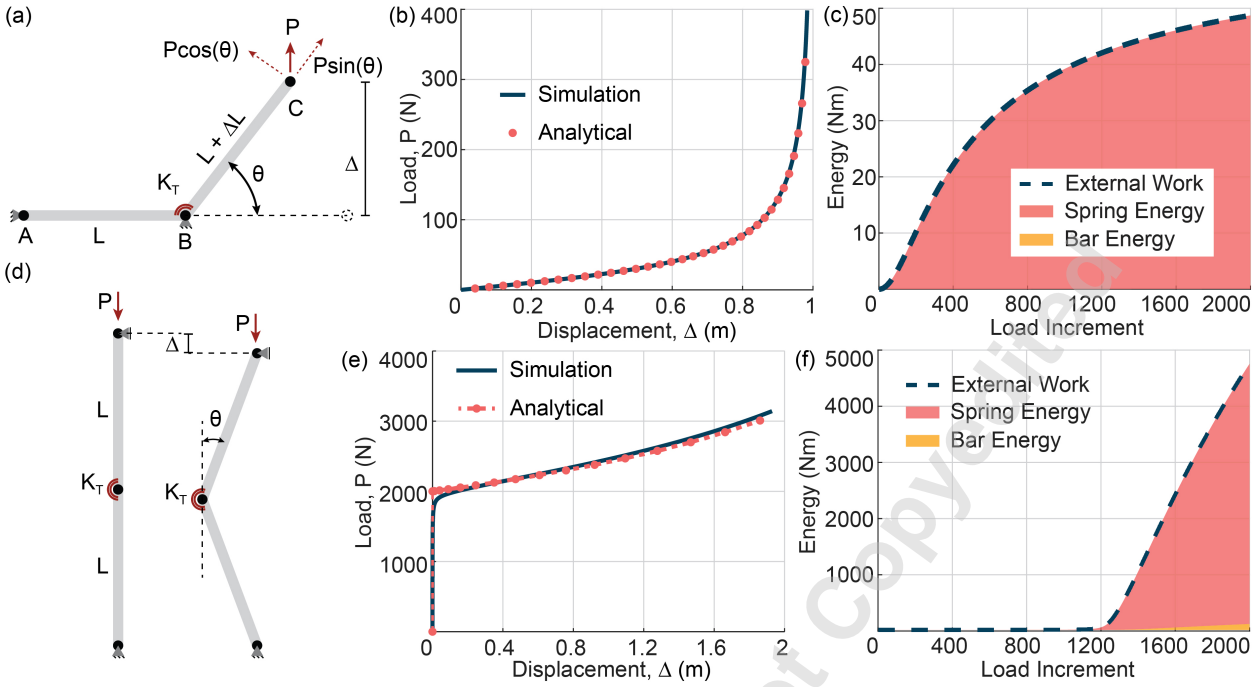

Fig. 2. Validation of the simulated behavior of bar-linked structures with torsional spring elements against their respective analytical solutions. (a) Simplest structure with a torsional spring element; (b) Comparison of analytical and simulated load–displacement responses for the structure in (a); (c) Simulated external work and stacked internal strain energies (spring and bars) over load increments for the structure in (a); (d) Buckling of a bar-linked vertical column comprising two bars and a torsional spring element at the central joint; (e) Comparison of analytical and simulated load–displacement responses for the structure in (d); (f) Simulated external work and stacked internal strain energies (spring and bars) over load increments for the structure in (d)

ness, the overall response visually appears to asymptote toward infinity in the load-displacement plot. Furthermore, as shown in Fig. 2 (c), there is excellent alignment between the work done by the external load and the cumulative strain energy stored in each element type, which confirms energy balance and validates the correct implementation of the torsional spring element within the nonlinear solver framework.

3.2 Comparing analytical and simulated buckling behavior of a vertical column structure

The vertical column structure shown in Fig. 2 (d) consists of two bars with a torsional spring element at the central joint. The bottom end of the column is fixed, while the top end is a roller support that restrains horizontal motion but allows vertical movement. The analytical relationship

between the load, P and bar rotation, θ can be obtained using potential energy analysis as

$$P = \frac{2K\theta}{L\sin(\theta)} \, . \tag{16}$$

The structure becomes unstable when the applied load reaches the critical value $P = 2K/L$. Thereafter, the column undergoes progressive deformation until each bar rotates by $\theta = \pi/2$, at which stage the load reaches $P = \pi K/L$, representing a fully folded configuration. The vertical displacement of the roller end beyond instability can be expressed as $\Delta = 2L(1 - \cos(\theta))$. It should be noted that the potential energy analysis assumes rigid bars, while the non-linear solver models the bars as linearly elastic. Consequently, slight differences are expected in the analytical and simulated buckling behavior of the vertical column.

In the simulation, the bars have a Young's modulus $E = 3 \times 10^9$ Pa, cross-sectional area $A = 1$ m^2, bar lengths $L = 1$ m, and torsional spring stiffness $K_T = 1000$ Nm/rad. A minor geometric imperfection is introduced at the free node to trigger the buckling behavior. As shown in Fig. 2 (e), the simulated structure exhibits instability at a load slightly lower than predicted analytically, due to elastic bar deformations and non-ideal buckling triggered with a geometric imperfection. After the onset of buckling, the load continues to increase till the bars rotate by $\theta = \pi/2$. Overall, the simulated load-displacement curve agrees well with the analytical prediction, capturing the same deformation trend and load magnitude, with minor deviations attributed to elastic bar effects and accumulated numerical drift at large displacements. Moreover, the close agreement between the work done by external loads and internal strain energies shown in Fig. 2 (f) validates the torsional spring element behavior within the non-linear solvers.

4 APPLICATION TO RECONFIGURABLE BAR-LINKED STRUCTURES

With the torsional spring element validated, the developed analysis program can now be extended to study load requirements for actuation and functional applications of reconfigurable bar-linked structures. Previous work by the authors introduced a systematic method to generate reconfigurable trusses from existing static truss designs and demonstrated their stability under design

Journal of Applied Mechanics. Received December 05, 2025;
Accepted manuscript posted January 12, 2026. doi:10.1115/1.4070821

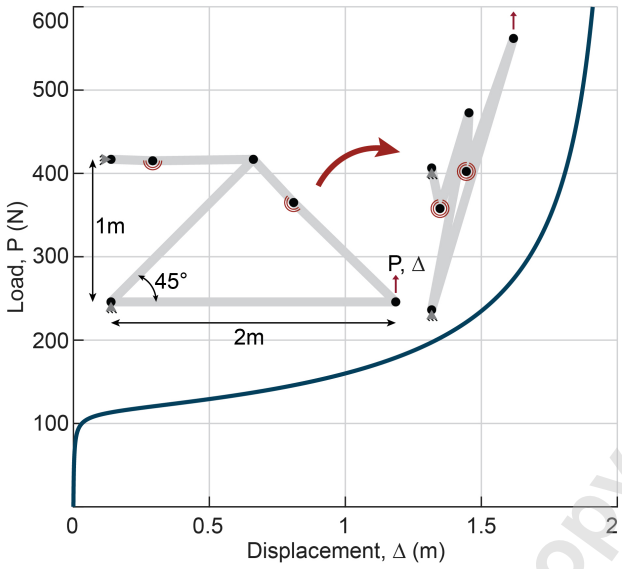

Fig. 3. Load analysis of the actuation of a reconfigurable cantilever truss

loading conditions [24]. These reconfigurable trusses can be fitted with torsional springs at their reconfigurable joints, enabling them to serve as functional systems capable of storing and releasing energy during load reversals.

The torsional spring implementation within the non-linear solver facilitates the simulation of load-displacement responses in such reconfigurable bar-linked systems. Incorporating torsional springs into these structures allows for the study of impact energy storage through spring strain energy, provided that the springs are locked after reaching their maximum deformation. This configuration also enables the evaluation of the stiffness associated with rotational joints and the estimation of actuation forces required to deploy or reconfigure the structure.

As a preliminary demonstration, a reconfigurable truss structure from our earlier work [24] is analyzed here to illustrate the potential application of the developed analysis program. The reconfigurable cantilever truss shown in Fig. 3 consists of bars with Young's modulus $E = 3 \times 10^6$ Pa, cross-sectional area $A = 0.5$ m^2, and torsional springs of stiffness $K_T = 50$ Nm/rad. The bar lengths are indicated in Fig. 3, and the reader is referred to Ref. [24] for the exact locations of the torsional springs.

This truss remains force-stable when loaded in the negative-Y direction. When the direction

of loading is reversed to induce reconfiguration, the analysis program can be used to evaluate the load-displacement response of the structure for various spring stiffnesses. Between the two orientations shown in Fig. 3, an actuation force of approximately 600 N was required to achieve reconfiguration. The resulting load-displacement curve reflects characteristics similar to those observed in the validation examples, exhibiting both spring deformation and buckling behavior, and also illustrates the amount of energy stored within the system due to the applied load. This stored energy can be harnessed for functional purposes when the structure is constrained from returning to its original configuration. With further development, the analysis framework may also enable sequential release of individual torsional springs, providing a mechanism for controlled or rapid deployment of reconfigurable structures.

5 CONCLUDING REMARKS

This technical note presented the formulation of a three-node torsional spring element stiffness matrix and validated its accuracy through comparison with analytical solutions of two benchmark examples. The torsional spring element successfully captured large-deformation responses and the onset of buckling in spring-fitted bar-linked structures. Finally, an example was included to demonstrate the capability of the developed analysis program to simulate actuation in reconfigurable bar-linked structures equipped with torsional springs. This example previews the potential of the model for the exploration of functional use cases of reconfigurable bar-linked structures. The solver implementation is made available as a matrix structural analysis program accompanying this note.

DATA ACCESSIBILITY

The torsional spring element implementation within a structural analysis program can be accessed at www.github.com/hardikyp/bar-linked-torsional-springs.

AUTHORS' CONTRIBUTIONS

Hardik Y. Patil: Methodology, Software, Validation, Formal Analysis, Investigation, Data Curation, Writing — Original Draft, Writing — Review & Editing, Visualization.

Evgueni T. Filipov: Conceptualization, Methodology, Validation, Resources, Writing — Review & Editing, Supervision, Project Administration, Funding Acquisition.

All authors gave final approval for publication and agreed to be held accountable for the work performed therein.

CONFLICT OF INTEREST DECLARATION

The authors declare that they have no known competing financial interests or personal relationships that could have appeared to influence the work reported in this paper.

ACKNOWLEDGEMENT

We acknowledge support from National Science Foundation (NSF) Grant Number: 1943723, and the Automotive Research Center (ARC) Cooperative Agreement W56HZV-19-2-0001. The paper reflects the views and opinions of the authors, and not necessarily those of the funding entities.

REFERENCES

[1] Felippa, C. A., 2001, "A historical outline of matrix structural analysis: A play in three acts," *Computers & Structures,* **79**(14), pp. 1313–1324.

[2] Kim, B., and Deshpande, A. D., 2014, "Design of nonlinear rotational stiffness using a non-circular pulley-spring mechanism," *Journal of Mechanisms and Robotics,* **6**(4), p. 041009.

[3] Franco, J. A., Gallego, J. A., and Herder, J. L., 2021, "Static balancing of four-bar compliant mechanisms with torsion springs by exerting negative stiffness using linear spring at the instant center of rotation," *Journal of Mechanisms and Robotics,* **13**(3), p. 031010.

[4] Knox, B. T., and Schmiedeler, J. P., 2009, "A unidirectional series-elastic actuator design using a spiral torsion spring," *Journal of Mechanical Design,* **131**(12).

[5] Dumas, C., Caro, S., Cherif, M., Garnier, S., and Furet, B., 2012, "Joint stiffness identification of industrial serial robots," *Robotica,* **30**(4), pp. 649–659.

[6] Edwards, W. T., 2007, "Effect of joint stiffness on standing stability," *Gait & Posture,* **25**(3), pp. 432–439.

[7] Fang, C., Ajoudani, A., Bicchi, A., and Tsagarakis, N. G., 2017, "Online model based estimation of complete joint stiffness of human arm," *IEEE Robotics and Automation Letters,* **3**(1), pp. 84–91.

[8] Gillman, A., Fuchi, K., and Buskohl, P., 2018, "Truss-based nonlinear mechanical analysis for origami structures exhibiting bifurcation and limit point instabilities," *International Journal of Solids and Structures,* **147**, pp. 80–93.

[9] Zhu, Y., Schenk, M., and Filipov, E. T., 2022, "A review on origami simulations: From kinematics, to mechanics, toward multiphysics," *Applied Mechanics Reviews,* **74**(3), p. 030801.

[10] Lu, L., Leanza, S., and Zhao, R. R., 2023, "Origami with rotational symmetry: A review on their mechanics and design," *Applied Mechanics Reviews,* **75**(5), p. 050801.

[11] Zhang, Y., Restrepo, D., Velay-Lizancos, M., Mankame, N. D., and Zavattieri, P. D., 2019, "Energy dissipation in functionally two-dimensional phase transforming cellular materials," *Scientific Reports,* **9**(1), p. 12581.

[12] Zhang, Y., Velay-Lizancos, M., Restrepo, D., Mankame, N. D., and Zavattieri, P. D., 2021, "Architected material analogs for shape memory alloys," *Matter,* **4**(6), pp. 1990–2012.

[13] Zhu, S., Tan, X., Chen, S., Wang, B., Ma, L., and Wu, L., 2020, "Quasi-all-directional negative stiffness metamaterials based on negative rotation stiffness elements," *physica status solidi (b),* **257**(6), p. 1900538.

[14] WASFY, T. M., 1996, "A torsional spring-like beam element for the dynamic analysis of flexible multibody systems," *International Journal for Numerical Methods in Engineering,* **39**(7), pp. 1079–1096.

[15] Kartal, M., Basaga, H., Bayraktar, A., and Muvafık, M., 2010, "Effects of semi-rigid connection on structural responses," *Electronic Journal of Structural Engineering,* **10**, pp. 22–35.

[16] Yao, H., Huang, Y., Ma, W., Liang, L., and Zhao, Y., 2023, "Dynamic analysis of a large

deployable space truss structure considering semi-rigid joints," *Aerospace,* **10**(9), p. 821.

[17] Molina-Villegas, J. C., and Ortega, J. E. B., 2023, "Closed-form solution of timoshenko frames with semi-rigid connections," In Structures, Vol. 48, Elsevier, pp. 212–225.

[18] Mohammed, D. R., and Ismael, M. A., 2019, "Effect of semi-rigid connection on post-buckling behaviour of frames using finite element method," *Civil Engineering Journal,* **5**(7), pp. 1619–1630.

[19] Schenk, M., Guest, S. D., et al., 2011, "Origami folding: A structural engineering approach," *Origami,* **5**, pp. 291–304.

[20] Liu, K., and Paulino, G. H., 2017, "Nonlinear mechanics of non-rigid origami: An efficient computational approach," *Proceedings of the Royal Society A: Mathematical, Physical and Engineering Sciences,* **473**(2206), p. 20170348.

[21] Filipov, E., Liu, K., Tachi, T., Schenk, M., and Paulino, G. H., 2017, "Bar and hinge models for scalable analysis of origami," *International Journal of Solids and Structures,* **124**, pp. 26–45.

[22] Woodruff, S. R., and Filipov, E. T., 2020, "A bar and hinge model formulation for structural analysis of curved-crease origami," *International Journal of Solids and Structures,* **204**, pp. 114–127.

[23] McGuire, W., Gallagher, R., and Ziemian, R., 2015, *Matrix Structural Analysis* Wiley.

[24] Patil, H. Y., and Filipov, E. T., 2025, Transforming static trusses into shape morphing systems using principles of quadrilateral linkages "View submitted manuscript at https://github.com/hardikyp/reconfigurable-trusses".

LIST OF FIGURES